

---

# Sculpting [CLS] Features for Pre-Trained Model-Based Class-Incremental Learning

---

**Murat Onur Yildirim**  
TU Eindhoven  
m.o.yildirim@tue.nl

**Elif Ceren Gok Yildirim**  
TU Eindhoven  
e.c.gok@tue.nl

**Joaquin Vanschoren**  
TU Eindhoven  
j.vanschoren@tue.nl

## Abstract

Class-incremental learning requires models to continually acquire knowledge of new classes without forgetting old ones. Although pre-trained models have demonstrated strong performance in class-incremental learning, they remain susceptible to catastrophic forgetting when learning new concepts. Excessive plasticity in the models breaks generalizability and causes forgetting, while strong stability results in insufficient adaptation to new classes. This necessitates effective adaptation with minimal modifications to preserve the general knowledge of pre-trained models. To address this challenge, we first introduce a new parameter-efficient fine-tuning module ‘Learn and Calibrate’, or LuCA, designed to acquire knowledge through an adapter-calibrator couple, enabling effective adaptation with well-refined feature representations. Second, for each learning session, we deploy a sparse LuCA module on top of the last [CLS] token just before the classifier, which we refer to as ‘Token-level Sparse Calibration and Adaptation’, or TOSCA. This strategic design improves the orthogonality between the modules and significantly reduces both training and inference complexity. By leaving the generalization capabilities of the pre-trained models intact and adapting exclusively via the last token, our approach achieves a harmonious balance between stability and plasticity. Extensive experiments demonstrate TOSCA’s state-of-the-art performance while introducing ~8 times fewer parameters compared to prior methods.

## 1 Introduction

Learning continuously from a series of concepts or classes using a unified model is a challenging problem due to *catastrophic forgetting* [1]—a phenomenon where the model’s performance on earlier concepts degrades as new classes are observed. Class-incremental learning (CIL) addresses this issue by enabling models to acquire knowledge from new classes while preserving their ability to correctly classify previously learned categories [2]. Until recently, most CIL methods have focused on relatively small networks such as ResNets [3] and often trained them from scratch with random initialization [4, 5]. With the rise of large Pre-Trained Models (PTMs) [6–8] such as Vision Transformers (ViTs) [9], many CIL methods now capitalize on the robust representations provided by PTMs, marking a significant paradigm shift in the field [10–17]. Specifically, several PTM-based CIL approaches [18–20] have demonstrated that strong initial representations, derived from large-scale pre-training, enhance incremental learning by enabling new classes to be learned with fewer training steps. However, sequential fine-tuning of the PTMs still changes their original representations and often leads to a substantial level of forgetting [21–23].

While parameter-efficient fine-tuning (PEFT) methods like prompts and adapters mitigate forgetting by restricting updates to small subsets of parameters, they introduce new trade-offs. Prompts maintain minimal adjustments on PTMs and offer great stability but often face challenges in adapting to specific tasks. In contrast, adapters provide localized feature refinement with high plasticity but this usually comes at the expense of quadratic parameter growth as the model depth increases. This leads us to an essential question in PTM-based CIL:

*How can we address the stability-plasticity dilemma [24] by unifying prompt-level stability and adapter-level plasticity, while maintaining efficient parameter scalability?*

To address this question, we first propose a new PEFT module ‘Learn and Calibrate’, or LuCA, which comprises two components: (1) a residual adapter that applies task-specific feature transformations, and (2) a calibrator that enhances discriminative features via attention-like gating. We then propose a novel module placement strategy that integrates a single LuCA module, operating exclusively on the final [CLS] token representation of ViTs. We term this approach ‘Token-level Sparse Calibration and Adaptation’, or shortly TOSCA. By localizing adaptations at the final semantic aggregation point, we preserve the PTM’s feature hierarchy: low/mid-level features remain frozen to maintain generalizability while final high-level abstractions adapt to a given task, akin to the harmony of ventral visual stream [25, 26] and prefrontal cortex [27–29].

Specifically, each increment is residually acquired by a dedicated LuCA module sparsified by  $\ell_1$ -regularization. This promotes parameter orthogonality and enhances module specialization or distinctiveness across modules. Inference protocol leverages entropy minimization over task-specific predictions, as correct modules produce low-entropy class distributions. This approach eliminates the need for task identifiers or exemplar replay while achieving state-of-the-art performance without complicated procedures.

Our contributions are three-fold:

- I. We introduce a PEFT module LuCA designed to learn task-specific residual transformations while refining features through additional calibration gating.
- II. We then propose TOSCA, a neuro-inspired and theoretically grounded PTM-based CIL approach that strategically integrates our LuCA module with a simple design. It effectively balances prompt-level stability and adapter-level plasticity while maintaining a model-agnostic parameter count, unlike many prompt- and adapter-based methods that scale linearly with the number of layers.
- III. We validate TOSCA’s advantages with extensive experiments on six benchmarks: (i) 7–21% higher accuracy than prompt-based methods and 4–12% higher than adapter-based methods on out-of-distribution datasets, (ii)  $\sim 2.5\times$  faster runtime, and (iii)  $\sim 8\times$  fewer parameters than layer-wise adapters in ViT-B/16.

## 2 Related Work

**CIL with Randomly Initialized Models.** Not a long time ago, the primary focus in CIL was training deep neural networks sequentially from scratch, with the goal of efficiently acquiring the knowledge of new classes while minimizing forgetting of previous ones. Common CIL strategies can be categorized into four main approaches: Regularization-based methods [30–33] maintain the model by selectively stabilizing changes in parameters or predictions. Replay-based methods approximate and reconstruct previously learned data distributions by either storing [34–42] or generating [43–47] samples from past experiences. Architecture-based methods [48–52] allocate distinct parameters and subspaces to different sets of classes. Parameter isolation methods utilize iterative pruning [53–56] or dynamic sparse training [57–60] to preserve key parameters. These strategies have laid the foundation for advancing CIL methodologies.

**CIL with Pre-trained Models.** In contrast, recent advancements in CIL research have shifted towards leveraging PTMs. Representations derived from pre-training have proven effective not only in facilitating knowledge transfer but also in mitigating catastrophic forgetting during the downstream continual learning [18, 19]. Additionally, pre-training on a large set of base classes enables incremental learning with minimal adaptations [20]. Therefore, methods in this context aim to improve performance with minimal additions while freezing the PTMs. L2P [12] borrows a technique from NLP by introducing a learnable prompt pool and selecting instance-specific prompts via a key-query matching selection mechanism to guide the PTMs response. DualPrompt [13] extends L2P by designing G-Prompt and E-Prompt, which encode task-invariant and task-specific instructions.

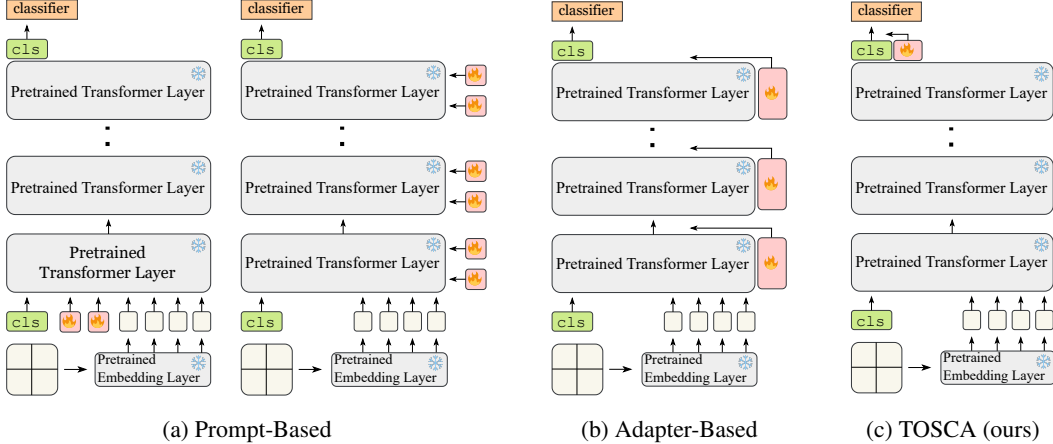


Figure 1: Prompt-based methods influence the self-attention process of a PTM, either from the input layer alone or across all layers. Adapter-based methods enable task-specific adaptations by inserting lightweight neural modules into the PTM’s layers. In contrast, we propose a single trainable module that operates exclusively on the final [CLS] token representation, efficiently adapting and calibrating features just before classification. This design offers a streamlined and effective alternative to both prompt- and adapter-based methods.

CODA-Prompt [14] uses contrastive learning to decorrelate representations of the prompts to reduce interference and combine them by attention-based weighting method. APER [15] explores various PEFT methods including adapters and shows that prototypical classifiers named SimpleCIL serve as a strong baseline. EASE [16] attaches adapters to each layer of PTMs to create expandable subspaces and during inference, it concatenates all feature representations from different sets of adapters to perform on a single classifier. MOS [17] adds replay generation for classifier alignment and an adapter merging over EASE to reduce mistakenly retrieving irrelevant modules during inference due to parameter drift.

### 3 Background

In this section, we first formally introduce the preliminaries of class-incremental learning and how pre-trained models are utilized to incrementally learn. We then present the overview of existing approaches using pre-trained models and their limitations.

#### 3.1 Class-Incremental Learning (CIL)

CIL is a learning scenario where a model continually learns to classify new classes to build a unified classifier [34]. Formally, we train models sequentially on a series of datasets  $\{D^1, D^2, \dots, D^B\}$  where  $D^b = \{(x_i, y_i)\}_{i=1}^{n_b}$  is the  $b$ -th training set with  $n_b$  instances. Within this setting, each training instance  $x_i \in \mathbb{R}^D$  is associated with a class  $y_i \in Y_b$ . Here,  $Y_b$  defines the set of labels for dataset  $b$ , and it is ensured that  $Y_b \cap Y_{b'} = \emptyset$  for any  $b \neq b'$ , i.e. non-overlapping classes for different datasets. During the  $b$ -th training stage, the model is updated using data exclusively from  $D_b$ .

From the model perspective, following typical PTM-based CIL works [12–17], we assume that a PTM is available for the initialization of the model  $f(\mathbf{x})$  which we define with two components:  $f(\mathbf{x}) = W^\top \phi(\mathbf{x})$ , where  $\phi(\cdot) : \mathbb{R}^D \rightarrow \mathbb{R}^d$  is the feature extractor and  $W \in \mathbb{R}^{d \times |\mathcal{Y}_b|}$  is the classifier. For a standard ViT [9], the initial encoding layer converts the image into a sequence of output features, denoted as  $\mathbf{x}_e \in \mathbb{R}^{L \times d}$ , where  $L$  is the sequence length. We simplify this by assuming [CLS] token is already prepended in  $\mathbf{x}_e$  as the first token. The sequence  $\mathbf{x}_e$  is then processed through subsequent layers, including multi-head self-attention and MLP, to produce the final embeddings. Finally, the embedded [CLS] token is considered as  $\phi(\mathbf{x})$ .

The effectiveness of the model is evaluated across all encountered classes, collectively represented as  $\mathcal{Y}_b = Y_1 \cup Y_2 \cup \dots \cup Y_b$ , after each learning stage. Specifically, we aim to find a model  $f(\mathbf{x}) : X \rightarrow \mathcal{Y}_b$  that minimizes empirical risk across all test dataset *without task indices* by balancing between learning new classes and retaining information about old ones in the *exemplar-free setting* [12–17].

### 3.2 Overview of PTM-Based CIL

In the era of PTMs, the main idea of many works seeks to modify the pre-trained weights slightly, to maintain the generalization strength and we can mainly divide these approaches into three.

**Learning Prototypical Classifiers.** These methods [11, 15] focus on learning a set of prototypical class representations, typically by computing class centroids or prototypes from the features of incremental classes. Given an input instance  $\mathbf{x}$  with label  $y \in \mathcal{Y}_b$ , let  $\phi(\mathbf{x})$  be its feature vector extracted by a pre-trained backbone. The class prototype  $\mathbf{p}_y$  is defined as in Eq. (1) and instances are classified by measuring their distance to these prototypes in the feature space. It is an efficient solution for simple class-incremental learning tasks by training only a classifier.

$$\mathbf{p}_y = \frac{1}{n_b} \sum_{i=1}^{n_b} \phi(\mathbf{x}_i) \quad (1)$$

However, these methods tend to rely too heavily on pre-trained knowledge and often fail to sufficiently adapt to new classes. This limits their effectiveness in more complex learning scenarios requiring feature-space reorganization.

**Learning Prompts.** This body of works [12–14] construct and train a learnable pool of prompts that can be shared across all tasks to influence the self-attention process either from the input layer alone or across all layers. This prompt pool with a size of  $M$  is denoted as  $\mathcal{P} = \{P_1, P_2, \dots, P_M\}$ , where  $P_j \in \mathbb{R}^{L_p \times d}$  represents a single prompt with token length  $L_p$  and the same embedding size  $d$  as image patch embedding  $\mathbf{x}_e$ . Each prompt is paired with a trainable key vector  $k_i \in \mathbb{R}^{d_k}$  encodes task-specific information while preserving the pre-trained backbone  $\phi(\cdot)$ , creating a set of key-prompt pairs  $\{(k_1, P_1), (k_2, P_2), \dots, (k_M, P_M)\}$ . The training objective jointly optimizes prompts, keys, and classifier through Eq. (2) where  $\ell(\cdot, \cdot)$  is cross-entropy loss measuring the discrepancy between the prediction and ground truth,  $\gamma(\cdot, \cdot)$  measures cosine similarity between keys and queries, and  $\lambda$  balances task performance against prompt selection efficacy.

$$\min_{\mathcal{P}, \mathcal{K}, \phi} \ell(W^\top \phi(\mathbf{x}; \mathcal{P}), y) + \lambda \sum_{i=1}^N \gamma(\phi(\mathbf{x}), k_{s_i}) \quad (2)$$

During inference, the model first extracts key features  $\phi(\mathbf{x})$  from the frozen backbone without any prompts to solve the prompt retrieval objective given in Eq. (3), selecting the top- $N$  prompts relevant to the input. These prompts then condition the transformer’s self-attention layers via concatenation with patch embeddings, yielding final predictions through the modified encoder  $\phi(\mathbf{x}; \mathcal{P})$ .

$$K_x^* = \arg \min_{\{s_i\}_{i=1}^N \subseteq [M]} \sum_{i=1}^N \gamma(\phi(\mathbf{x}), k_{s_i}), \quad (3)$$

Although they present relatively efficient adaptations, selecting the correct prompt for a given task becomes challenging especially in long and complex scenarios, as the fixed key embedding space  $\phi(\cdot)$  struggles to discriminate between semantically similar but task-distinct prompts, leading to retrieval conflicts when  $\gamma(k_i, k_j) \approx 1$  for prompts  $P_i, P_j$  from incompatible tasks, resulting in forgetting.

**Learning Adapters.** These approaches [15–17] address catastrophic forgetting by inserting lightweight neural modules called adapters into the PTM’s layers, enabling task-specific adaptations while preserving frozen base parameters. Each set of adapters  $\mathcal{A}_b = \{A_1, A_2, \dots, A_N\}$  for task  $b$  operates via residual connections on  $N$  number of transformer layers, typically projecting features through a low-dimensional bottleneck given an intermediate feature  $\mathbf{x}_i$  as in Eq. (4) where  $\mathbf{z}$  is usually the output of MLP block of a transformer layer and  $(r \ll d)$  form the adapter’s projection layers, and  $\sigma$  denotes a non-linear activation. This residual formulation allows gradual feature adaptation without destabilizing the PTM’s original representations.

$$A(\mathbf{z}) = \sigma(\mathbf{z}W_{down})W_{up} + \mathbf{z}, \quad W_{down} \in \mathbb{R}^{d \times r}, W_{up} \in \mathbb{R}^{r \times d} \quad (4)$$

Task-specific adapter sets then can be trained using either a feature concatenation strategy or a module merging strategy. Under the feature concatenation strategy, adapter sets are trained sequentially for each session and their outputs are concatenated with the PTM features at the cost of quadratic scaling or a linear increase in dimensionality. In contrast, the module merging strategy builds on previous adapter sets where each new set  $\mathcal{A}_b$  refines the representation produced by the preceding set  $\mathcal{A}_{b-1}$  to produce a gradual and unified feature representation. This is more parameter-efficient compared to the feature concatenation strategy but it risks accumulating feature drift over successive tasks, especially when new class distributions diverge significantly from those of earlier sessions.

Although adapter-based methods offer an architectural advantage such as not being limited to input token spaces, they modify the pre-trained model’s feature representations via residual additions. These modifications introduce subtle yet cumulative deviations from the original pre-trained feature space, particularly more pronounced in deeper layers. The standard practice of inserting adapters into all  $N$  transformer layers incurs substantial parameter overhead by requiring  $(B \times N \times 2dr)$  additional parameters where  $B$  denotes the number of tasks,  $r$  is the bottleneck projection dimension and  $d$  is the embedding size. Consequently, while individual adapters remain lightweight, their pervasive placement across layers and tasks challenges overall parameter efficiency during both training and inference.

## 4 Methodology

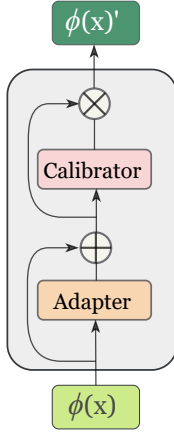


Figure 2: LuCA.

**LuCA Module.** It decouples feature transformation from discriminative feature enhancement with the dual adapter-calibrator architecture, allowing precise control over parameter updates. LuCA can process any intermediate representation  $\mathbf{z} \in \mathbb{R}^d$  through two sequential operations:

$$L(\mathbf{z}) = C(A(\mathbf{z})), \quad (5)$$

where  $A(\cdot)$  is a residual adapter that applies bottlenecked feature modulation with Eq. (4) to preserve original semantics via skip connections while learning task-specific offsets. The calibrator  $C(\cdot)$  then enhances adapted features through an attention-like gating, similar to the squeeze-and-excitation blocks [61], and refines more discriminative features with Eq. (6) where  $\odot$  denotes the Hadamard product. Compared to full fine-tuning which scales with  $\mathcal{O}(d^2)$ , LuCA provides an efficient and flexible mechanism for task adaptation with only  $4 \times d \times r$  trainable parameters, leading to a significantly reduced  $\mathcal{O}(dr)$  complexity, where  $r \ll d$ .

$$C(\mathbf{z}) = \mathbf{z} \odot \sigma(\mathbf{z}V_{down})V_{up}, \quad V_{down} \in \mathbb{R}^{d \times r}, V_{up} \in \mathbb{R}^{r \times d} \quad (6)$$

**TOSCA: Specialization for CIL.** We instantiate the LuCA module as TOSCA which is a strategic implementation for CIL that operates exclusively on the final [CLS] token of ViTs. Given an input  $\mathbf{x}$ , the frozen pre-trained backbone  $\phi(\cdot)$  generates  $\phi(\mathbf{x})$  which TOSCA refines through Eq. (7). The design of placing it at the last [CLS] token is a deliberate architectural choice with three advantages:

$$\phi(\mathbf{x})' = L(\phi(\mathbf{x})) = C(A(\phi(\mathbf{x}))) \quad (7)$$

First, by localizing adaptations to the final semantic aggregation point (the [CLS] token), TOSCA preserves the model’s feature hierarchy where low/mid-level features remain stable while the final high-level abstractions adapt to new tasks. This way, the intact PTM maintains its generalization and out-of-distribution robustness—a critical advantage over adapter-based methods that indirectly perturb intermediate representations through input and intermediate layer modifications.

Second, the [CLS] token inherently aggregates global semantic information, making it an optimal locus for task-specific refinement, in contrast to input-layer modifications of prompt-based approaches which indirectly influence later representations through the transformer’s self-attention mechanism.

Third, the total parameter count remains architecture-agnostic with  $4dr$  regardless of model depth, contrasting sharply with layer-wise adapters that scale linearly as  $N \times 2dr$  for  $N$  number of layers. This significant reduction in parameters leads to decreased training and inference complexity.

**Training Protocol.** We completely freeze the PTM  $\phi(\cdot)$  and only train the TOSCA’s parameters  $\Theta_B = \{W_{down}, W_{up}, V_{down}, V_{up}\}$  together with the prototypical classifier  $W^\top$ . We utilize a new TOSCA module for each incremental stage  $b$  which lets the model encode task-specific information in these lightweight modules by optimizing a composite objective function that combines cross-entropy loss with  $\ell_1$ -regularization as in Eq. (8) where  $\lambda$  controls the regularization strength.

$$\min_{\Theta_b \cup W} \sum_{(\mathbf{x}, y) \in \mathcal{D}^b} \ell_{CE}(W^\top \phi(\mathbf{x})', y) + \lambda \|\Theta_b\|_1, \quad \phi(\mathbf{x})' = L(\phi(\mathbf{x})) \quad (8)$$

The  $\ell_1$  term induces sparsity in the parameters, encouraging orthogonal configurations across different tasks. This orthogonal specialization enables each module to focus on distinct feature dimensions, preventing interference between successive tasks [62, 63]. After training, we store  $B$  while keeping the pre-trained backbone  $\phi(\cdot)$  immutable.

**Inference Protocol.** During inference, we first extract the frozen backbone’s representation  $\phi(\mathbf{x})$  through a single forward pass to ensure computational efficiency. This shared feature vector is then easily processed by all TOSCA modules and each transformed feature  $\phi(\mathbf{x})'_b$  then generates task-specific probability distributions. The final prediction is selected through entropy minimization over the union of all class probabilities as in Eq. (9) where  $H(\cdot)$  computes the Shannon entropy and  $\pi_b$  represents task priors (uniform by default). This entropy-based selection criterion leverages the observation that the correct task-specific module produces predictions with lower uncertainty due to its specialized feature calibration.

$$\hat{y} = \arg \min_{y \in \mathcal{Y}_b} H \left( \sum_{b=1}^B \pi_b p_b(y|\mathbf{x}) \right), \quad p_b(y|\mathbf{x}) = \text{softmax}(W^\top \phi(\mathbf{x})'_b) \quad (9)$$

**Theoretical Underpinnings.** In this approach, we focus adaptation solely on the final [CLS] token before classification, while ensuring that the feature manifolds of all preceding layers remain unchanged. Specifically, the design of TOSCA guarantees that, for all layers  $n < N$ , the feature manifolds  $\mathcal{H}_n$  of the PTM are preserved as in Eq. (10), meaning the feature distributions remain identical to the PTM’s distributions up to the penultimate layer. This stability ensures that the model retains the learned features from prior tasks, avoiding catastrophic forgetting.

$$\forall n < N : \mathcal{H}_n^{TOSCA} = \mathcal{H}_n^{PTM} \quad (10)$$

By adapting exclusively through [CLS] of the final layer  $N$ , we achieve a controlled adjustment by allowing a small, bounded deviation in the feature manifold at this layer while maintaining backward compatibility with previously learned classes. The bounded deviation is formally expressed as in Eq. (11) where  $\epsilon$  is a small value controlled by the residual connection, that limits the change in the feature space and does not disrupt the learned knowledge.

$$\gamma(\mathcal{H}_N^{PTM}, \mathcal{H}_N^{TOSCA}) \leq \epsilon \quad (11)$$

**Neuroscientific Inspirations.** The brain’s continual learning ability arises from encoding invariant representations in the ventral visual stream [25, 26] and flexibly adapting them via task-specific circuits in the prefrontal cortex [27–29]. In other words, the prefrontal cortex receives invariant visual information from the ventral stream and refines these representations through selective synaptic plasticity to adapt to current behavioral demands. This enables the cortex to manipulate and utilize these representations to guide final behavior effectively. Inspired by this, our method leverages a pre-trained ViT to emulate the ventral visual stream’s stable and invariant feature extraction and employs lightweight modules just before the decision-making, analogous to flexible cortical circuits that tailor general representations for specific tasks. This approach not only minimizes the need to relearn basic features for each new task but also mirrors the brain’s learning principles.

**Summary.** Prompts effectively modulate the self-attention mechanism without explicitly adding new representations, thereby enhancing stability. Conversely, adapters facilitate adaptation to new classes by subtly modifying the PTM’s feature representations via residual additions, which enhances plasticity. To combine these complementary advantages, we introduce a new PEFT module LuCA that integrates an adapter with a calibrator to produce refined feature representations. Unlike many PTM-based CIL methods that place modules at every layer, we strategically position a sparse LuCA module to operate solely on the final [CLS] token just before the classifier, which we refer to as TOSCA. This design enables the orthogonal specialization of modules to focus on distinct feature dimensions, prevents interference between tasks during inference, and efficiently strikes the balance between stability and plasticity in continual learning without compromising the PTM’s generalization.

## 5 Experiments

In this section, we describe the experimental setup and present experiments conducted on six different benchmarks to evaluate the incremental learning capabilities of TOSCA, in comparison with other state-of-the-art algorithms. Additionally, we share a parameter and run-time analysis as well as an ablation study to provide the robustness of the proposed method more in detail. Please see our Appendix A.1 for more details.

### 5.1 Experimental Setup

**Datasets.** Since PTMs often exhibit substantial knowledge of upstream tasks, we adopt the evaluation framework proposed in [12–17] to assess their performance across a diverse set of benchmarks. These include CIFAR-100 [64], CUB-200 [65], ImageNet-R [66] ImageNet-A [67], OmniBenchmark [68], and VTAB [69]. These datasets encompass both standard CIL benchmarks and out-of-distribution datasets which exhibit significant domain shifts relative to the dataset used for pre-training (e.g. ImageNet [70]). Specifically, the datasets vary in scale: CIFAR-100 has 100 classes of natural images, each with 500 training images. CUB-200 dataset consists of images from 200 bird classes, with about 30 images per class for training. ImageNet-R includes 24000 for training images from 200 classes with abstract forms. ImageNet-A consists of 200 classes and 7500 training samples that are usually misclassified by ResNet models. Omnibenchmark with 300 classes and VTAB with 100 classes are designed to evaluate the generalization of visual representations.

**Dataset Splits.** Following [15–17], we use the notation ‘B- $m$  Inc- $n$ ’ to represent the class splits, where  $m$  specifies the number of classes in the initial stage and  $n$  denotes the number of classes added at each incremental stage. Consistent with [34], we shuffle the class order randomly using the seed 1993 before splitting the data. To ensure a fair comparison, the training and testing sets for all methods are maintained the same.

**Comparison Methods.** We select state-of-the-art PTM-based CIL methods for comparison, including SimpleCIL [15], L2P [12], DualPrompt [13], CODA-Prompt [14], APER [15], EASE [16] and MOS [17]. We also include one lower-bound and one upper-bound reference point: ‘Finetune’ sequentially fine-tunes the PTM; and ‘joint’ trains the model with all classes at the same time. All methods are implemented using the same PTM for consistency.

**Evaluation Metrics.** We compare the methods based on the accuracy over all stages obtained after last stage and the accuracy across all stages. Formally, building on [34], we denote the Top-1 accuracy after the  $b$ -th stage as  $\mathcal{A}_b$  and use  $\mathcal{A}_B$  to represent the performance after the final stage. The average performance across all incremental stages then measured by  $\bar{\mathcal{A}} = \frac{1}{B} \sum_{b=1}^B \mathcal{A}_b$ .

**Implementation Details.** We conduct our experiments on an NVIDIA A100, and reproduce the compared methods using PyTorch [71] and Pilot [72]. Consistent with [15–17], we utilize two representative pre-trained models: ViT-B/16-IN21K and ViT-B/16-IN1K. Both models are pre-trained on ImageNet21K, with the latter further fine-tuned on ImageNet1K. For TOSCA, we train the model using the SGD optimizer with a batch size of 48 over 20 epochs. The learning rate starts at 0.025 and follows a cosine annealing schedule. The projection dimension  $r$  is set to 48 and the  $\ell_1$  contribution  $\lambda$  is set to 0.0005. We perform multiple runs with five different random seeds and report mean and standard deviation for each method.

Table 1: Average and last accuracy [%] performance on six datasets with **ViT-B/16-IN21K** as the backbone. ‘IN-R/A’ stands for ‘ImageNet-R/A,’ and ‘OmniBench’ stands for ‘OmniBenchmark.’ We report all compared methods with their source code and show the best performance in bold.

Method	CIFAR B0 Inc5		CUB B0 Inc10		IN-R B0 Inc20		IN-A B0 Inc20		OmniBench B0 Inc30		VTAB B0 Inc10	
	$\bar{A}$	$\mathcal{A}_B$	$\bar{A}$	$\mathcal{A}_B$	$\bar{A}$	$\mathcal{A}_B$	$\bar{A}$	$\mathcal{A}_B$	$\bar{A}$	$\mathcal{A}_B$	$\bar{A}$	$\mathcal{A}_B$
Joint	–	96.21 $\pm$ 1.0	–	92.62 $\pm$ 1.1	–	81.92 $\pm$ 1.4	–	67.97 $\pm$ 1.9	–	85.44 $\pm$ 1.2	–	94.96 $\pm$ 1.2
Finetune	60.65 $\pm$ 5.6	48.12 $\pm$ 3.3	55.78 $\pm$ 2.8	33.13 $\pm$ 3.3	59.09 $\pm$ 3.7	49.46 $\pm$ 3.3	30.98 $\pm$ 3.4	19.86 $\pm$ 1.8	63.71 $\pm$ 1.0	45.45 $\pm$ 1.0	31.60 $\pm$ 6.0	21.63 $\pm$ 8.3
SimpleCIL	86.48 $\pm$ 0.8	81.28 $\pm$ 0.1	91.58 $\pm$ 1.3	86.73 $\pm$ 0.1	61.31 $\pm$ 0.4	54.55 $\pm$ 0.1	58.92 $\pm$ 1.0	48.77 $\pm$ 0.1	79.59 $\pm$ 1.5	73.13 $\pm$ 0.1	90.65 $\pm$ 1.1	84.43 $\pm$ 0.1
L2P	84.90 $\pm$ 1.2	80.06 $\pm$ 1.4	73.22 $\pm$ 1.8	61.55 $\pm$ 1.7	75.92 $\pm$ 0.7	70.88 $\pm$ 0.7	50.13 $\pm$ 1.8	42.80 $\pm$ 1.1	73.96 $\pm$ 2.0	64.63 $\pm$ 0.6	78.61 $\pm$ 4.2	64.81 $\pm$ 2.9
DualPrompt	85.61 $\pm$ 1.3	79.92 $\pm$ 0.4	81.36 $\pm$ 1.8	70.51 $\pm$ 1.1	71.48 $\pm$ 0.5	66.09 $\pm$ 1.3	51.57 $\pm$ 0.4	40.56 $\pm$ 1.6	75.58 $\pm$ 1.4	66.46 $\pm$ 0.8	86.86 $\pm$ 2.8	75.86 $\pm$ 3.7
CODA-Prompt	87.64 $\pm$ 0.4	81.46 $\pm$ 0.3	77.65 $\pm$ 1.0	68.44 $\pm$ 1.0	76.25 $\pm$ 0.3	71.39 $\pm$ 0.3	58.82 $\pm$ 0.78	47.18 $\pm$ 0.9	73.73 $\pm$ 0.5	69.46 $\pm$ 0.7	87.60 $\pm$ 0.5	86.71 $\pm$ 0.8
APER-Adapter	89.57 $\pm$ 0.9	84.91 $\pm$ 0.2	91.62 $\pm$ 1.2	86.72 $\pm$ 0.2	74.81 $\pm$ 0.8	66.97 $\pm$ 0.8	59.57 $\pm$ 1.6	49.46 $\pm$ 0.4	80.48 $\pm$ 1.2	74.04 $\pm$ 0.3	90.59 $\pm$ 1.0	84.28 $\pm$ 0.2
EASE	90.79 $\pm$ 0.8	85.97 $\pm$ 0.6	92.51 $\pm$ 1.3	86.49 $\pm$ 1.2	80.35 $\pm$ 1.0	75.74 $\pm$ 0.8	64.00 $\pm$ 1.5	54.99 $\pm$ 1.0	81.11 $\pm$ 0.8	74.16 $\pm$ 2.0	90.26 $\pm$ 3.6	82.07 $\pm$ 3.0
MOS	93.45 $\pm$ 0.9	90.04 $\pm$ 0.6	93.42 $\pm$ 1.2	90.07 $\pm$ 0.9	82.26 $\pm$ 1.0	77.62 $\pm$ 0.9	63.57 $\pm$ 2.0	54.60 $\pm$ 0.8	84.73 $\pm$ 1.1	79.97 $\pm$ 0.9	92.75 $\pm$ 1.0	92.74 $\pm$ 0.9
TOSCA (ours)	<b>96.37</b> $\pm$ 0.5	<b>95.64</b> $\pm$ 0.8	<b>93.47</b> $\pm$ 1.9	<b>91.09</b> $\pm$ 1.8	<b>82.27</b> $\pm$ 1.9	<b>78.28</b> $\pm$ 1.9	<b>66.92</b> $\pm$ 3.0	<b>65.37</b> $\pm$ 2.9	<b>84.75</b> $\pm$ 2.6	<b>82.35</b> $\pm$ 1.0	<b>96.59</b> $\pm$ 1.6	<b>93.87</b> $\pm$ 2.0

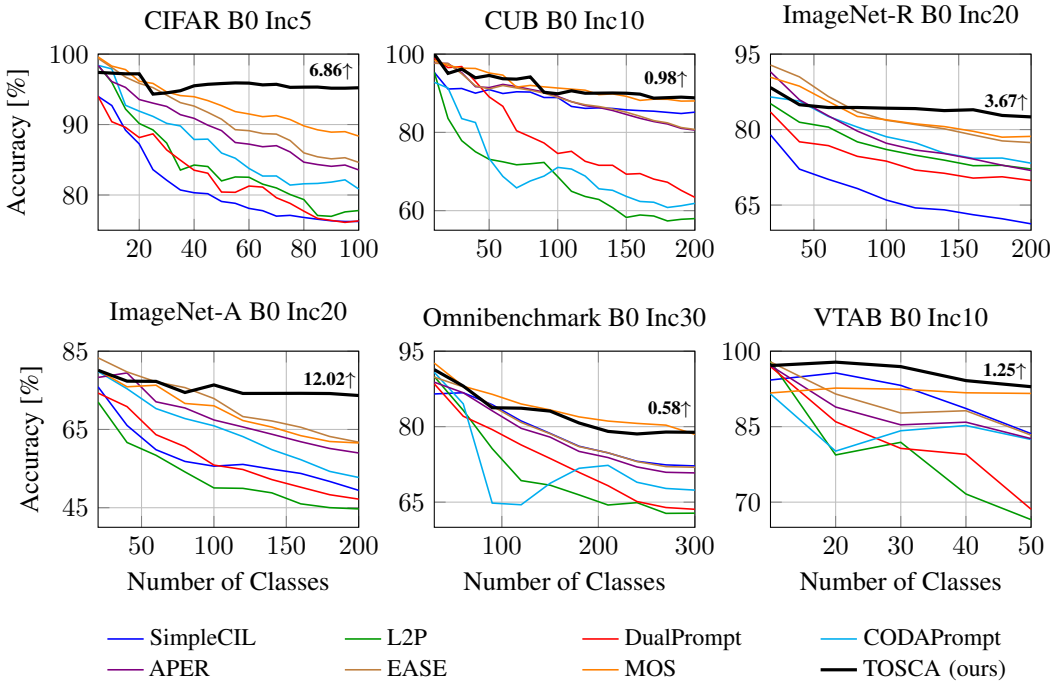


Figure 3: Performance curve of different methods under different settings. All methods are initialized with **ViT-B/16-IN1K**. We annotate the relative improvement of TOSCA above the runner-up method with numerical numbers at the last incremental stage.

## 5.2 State-of-the-art Comparison

In this section, we compare TOSCA to other state-of-the-art methods on six benchmark datasets and different pre-trained backbones. Table 1 reports the accuracy after the final learning stage with ViT-B/16-IN21K for different methods. Our approach achieves the best performance among all six benchmarks, substantially outperforming the current state-of-the-art methods, i.e. EASE, and MOS which is *not* completely exemplar-free due to replay generation for classifier alignment. We also report the incremental performance trend over the training sessions for different methods in Figure 3. We find TOSCA outperforms the runner-up method by 4% – 12% on CIFAR100, ImageNet-R, and ImageNet-A as highlighted in the annotations at the end of each image. Additionally, we also compare TOSCA with a traditional 100-epoch joint training as an upper-bound. Although joint training still leads, our approach remains highly close and demonstrates competitive performance by training only a single lightweight module per task. These results indicate that TOSCA is a versatile approach, effective in enhancing performance with various backbones. Please see our Appendix A.2 for more experimental results.



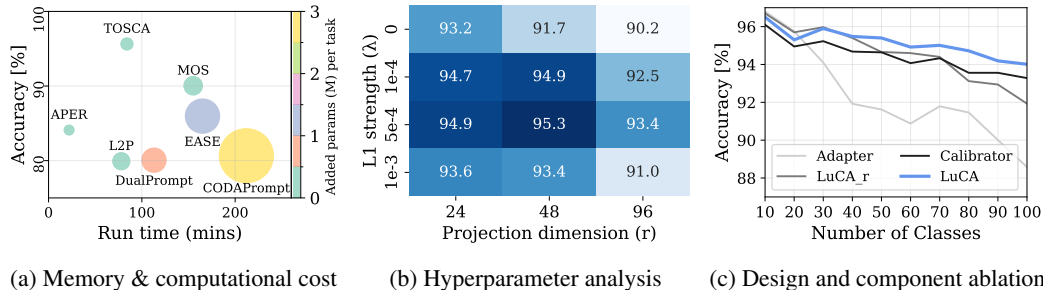


Figure 4: Performance evaluation of TOSCA across different perspectives. (a) Memory & computational cost highlights TOSCA’s efficiency, (b) Hyperparameter analysis illustrates effect of  $\ell_1$  strength ( $\lambda$ ) and projection dimension ( $r$ ) on accuracy, (c) Design and component ablation presents the impact of different components and flows on accuracy.

### 5.3 Parameter and Run-Time Analysis

We further investigate PTM-based CIL approaches in terms of accuracy, computational cost (run time), and parameter efficiency on CIFAR B0 Inc5 benchmark in Figure 4a. TOSCA achieves the top performance while maintaining a low computational cost and parameter overhead per task. In contrast, methods like CODA-Prompt and EASE require significantly more parameters and longer run times, making them less efficient. Notably, MOS also attains high accuracy, but it comes at a higher computational expense due to additional processes such as adapter merging and replay generation. Overall, TOSCA demonstrates its effectiveness in CIL with minimal parameter overhead and shorter run-time, striking a balance between efficiency and performance.

### 5.4 Ablation Study

We also perform an ablation study on CIFAR B0 Inc10, evaluating the incremental performance across different learning settings. First, we analyze the impact of  $\ell_1$ -regularization strength ( $\lambda$ ) and projection dimension ( $r$ ) on performance, as shown in Figure 4b. Our findings indicate that moderate  $\ell_1$  regularization enhances accuracy, with performance peaking at  $\lambda = 5e^{-4}$ . This promotes the orthogonality among different modules, improving module selection during inference. However, excessive sparsity degrades performance by excessively constraining representations, thereby reducing expressiveness and learning capacity. Similarly, increasing the projection dimension ( $r$ ) improves accuracy up to  $r = 48$ , beyond which performance deteriorates due to the larger bottleneck. Based on these observations, we identify the optimal configuration as  $\lambda = 5e^{-4}$  and  $r = 48$ , achieving an accuracy of 95.3%. Additionally, we compare the performance of different components, alternative module designs and configurations against LuCA in Figure 4c. This includes a reversed variant, LuCA\_r, which integrates new information atop the calibrated pre-trained features, formulated as  $\phi(\mathbf{x})' = A(C(\phi(\mathbf{x})))$ . Our results highlight the crucial role of the calibrator while LuCA surpasses other design variants by effectively harmonizing its two modules working together.

## 6 Conclusions

In this paper, we first introduce a new parameter efficient fine tuning module LuCA that enhances acquired knowledge by combining an adapter with a calibrator, thereby adapting to new information with well-refined features. Second, we propose a novel PTM-based CIL approach TOSCA which employs a single, sparse LuCA module that operates solely on the final [CLS] token before the classifier, enabling efficient and orthogonal task adaptation. Our approach consistently outperforms state-of-the-art methods by effectively navigating the stability-plasticity trade-off, while introducing significantly fewer parameters and overhead costs.

**Limitations and future works.** Possible limitations include the utilization of pre-trained models since it highly relies on the generalization strength of the pre-trained models by adapting through a single token only. In future work, we aim to explore further application scenarios, such as few-shot class-incremental learning to further enhance its versatility and impact.

## Broader Impact

This paper presents a work whose goal is to advance the field of machine learning, especially on the subject of exemplar-free class-incremental learning. Besides the advancements in the field, it eliminates the need to store data by introducing lightweight single trainable module, thereby diminishing privacy, memory, computation, and scalability concerns.

## Acknowledgements

This work is supported by TAILOR, a project funded by the EU Horizon programme under GA No. 952215; SYNERGIES, a project funded by the EU Horizon programme under GA No. 101146542; and Dutch e-infrastructure with the support of SURF Cooperative using GA no. EINF-10242.

## References

- [1] Michael McCloskey and Neal J Cohen. Catastrophic interference in connectionist networks: The sequential learning problem. In *Psychology of learning and motivation*. Elsevier, 1989.
- [2] Marc Masana, Xialei Liu, Bartłomiej Twardowski, Mikel Menta, Andrew D Bagdanov, and Joost Van De Weijer. Class-incremental learning: survey and performance evaluation on image classification. *TPAMI*, 2022.
- [3] Kaiming He, Xiangyu Zhang, Shaoqing Ren, and Jian Sun. Deep residual learning for image recognition. In *CVPR*, 2016.
- [4] Da-Wei Zhou, Qi-Wei Wang, Zhi-Hong Qi, Han-Jia Ye, De-Chuan Zhan, and Ziwei Liu. Class-incremental learning: A survey. *TPAMI*, 2024.
- [5] Matthias De Lange, Rahaf Aljundi, Marc Masana, Sarah Parisot, Xu Jia, Aleš Leonardis, Gregory Slabaugh, and Tinne Tuytelaars. A continual learning survey: Defying forgetting in classification tasks. *TPAMI*, 2021.
- [6] Ze Liu, Yutong Lin, Yue Cao, Han Hu, Yixuan Wei, Zheng Zhang, Stephen Lin, and Baining Guo. Swin transformer: Hierarchical vision transformer using shifted windows. In *ICCV*, 2021.
- [7] Stéphane d’Ascoli, Hugo Touvron, Matthew L Leavitt, Ari S Morcos, Giulio Biroli, and Levent Sagun. Convit: Improving vision transformers with soft convolutional inductive biases. In *ICML*, 2021.
- [8] Alec Radford, Jong Wook Kim, Chris Hallacy, Aditya Ramesh, Gabriel Goh, Sandhini Agarwal, Girish Sastry, Amanda Askell, Pamela Mishkin, Jack Clark, et al. Learning transferable visual models from natural language supervision. In *ICML*, 2021.
- [9] Alexey Dosovitskiy, Lucas Beyer, Alexander Kolesnikov, et al. An image is worth 16x16 words: Transformers for image recognition at scale. In *ICLR*, 2021.
- [10] Yabin Wang, Zhiwu Huang, and Xiaopeng Hong. S-prompts learning with pre-trained transformers: An occam’s razor for domain incremental learning. 2022.
- [11] Paul Janson, Wenxuan Zhang, Rahaf Aljundi, and Mohamed Elhoseiny. A simple baseline that questions the use of pretrained-models in continual learning. *NeurIPS Workshop on Distribution Shifts*, 2022.
- [12] Zifeng Wang, Zizhao Zhang, Chen-Yu Lee, Han Zhang, Ruoxi Sun, Xiaoqi Ren, Guolong Su, Vincent Perot, Jennifer Dy, and Tomas Pfister. Learning to prompt for continual learning. In *CVPR*, 2022.
- [13] Zifeng Wang, Zizhao Zhang, Sayna Ebrahimi, et al. Dualprompt: Complementary prompting for rehearsal-free continual learning. In *ECCV*, 2022.
- [14] James Seale Smith, Leonid Karlinsky, Vyshnavi Gutta, et al. Coda-prompt: Continual decomposed attention-based prompting for rehearsal-free continual learning. In *CVPR*, 2023.
- [15] Da-Wei Zhou, Zi-Wen Cai, Han-Jia Ye, De-Chuan Zhan, and Ziwei Liu. Revisiting class-incremental learning with pre-trained models: Generalizability and adaptivity are all you need. *IJCV*, 2024.
- [16] Da-Wei Zhou, Hai-Long Sun, Han-Jia Ye, and De-Chuan Zhan. Expandable subspace ensemble for pre-trained model-based class-incremental learning. In *CVPR*, 2024.

- [17] Hai-Long Sun, Da-Wei Zhou, Hanbin Zhao, Le Gan, De-Chuan Zhan, and Han-Jia Ye. Mos: Model surgery for pre-trained model-based class-incremental learning. In *AAAI*, 2024.
- [18] Vinay Venkatesh Ramasesh, Aitor Lewkowycz, and Ethan Dyer. Effect of scale on catastrophic forgetting in neural networks. In *ICLR*, 2022.
- [19] Sanket Vaibhav Mehta, Darshan Patil, Sarath Chandar, and Emma Strubell. An empirical investigation of the role of pre-training in lifelong learning. *JMLR*, 24(214), 2023.
- [20] Tz-Ying Wu, Gurumurthy Swaminathan, Zhizhong Li, Avinash Ravichandran, Nuno Vasconcelos, Rahul Bhotika, and Stefano Soatto. Class-incremental learning with strong pre-trained models. In *CVPR*, 2022.
- [21] Mark D McDonnell, Dong Gong, Amin Parvaneh, Ehsan Abbasnejad, and Anton van den Hengel. Ranpac: Random projections and pre-trained models for continual learning. In *NeurIPS*, 2024.
- [22] Aristeidis Panos, Yuriko Kobe, Daniel Olmeda Reino, Rahaf Aljundi, and Richard E Turner. First session adaptation: A strong replay-free baseline for class-incremental learning. In *ICCV*, 2023.
- [23] Gengwei Zhang, Liyuan Wang, Guoliang Kang, Ling Chen, and Yunchao Wei. Slca: Slow learner with classifier alignment for continual learning on a pre-trained model. In *ICCV*, 2023.
- [24] Stephen T Grossberg. *Studies of mind and brain: Neural principles of learning, perception, development, cognition, and motor control*. Springer Science & Business Media, 2012.
- [25] Irving Biederman and Peter C Gerhardstein. Recognizing depth-rotated objects: evidence and conditions for three-dimensional viewpoint invariance. *Journal of Experimental Psychology: Human perception and performance*, 19(6):1162, 1993.
- [26] Irving Biederman. Recognition-by-components: a theory of human image understanding. *Psychological review*, 94(2):115, 1987.
- [27] Ningyu Zhang and Ning-long Xu. Reshaping sensory representations by task-specific brain states: Toward cortical circuit mechanisms. *Current Opinion in Neurobiology*, 77:102628, 2022.
- [28] Karl Friston and Stefan Kiebel. Cortical circuits for perceptual inference. *Neural Networks*, 22(8):1093–1104, 2009.
- [29] Apoorva Bhandari, Haley Keglovits, and David Badre. Task structure tailors the geometry of neural representations in human lateral prefrontal cortex. *bioRxiv*, 2024.
- [30] James Kirkpatrick et al. Overcoming catastrophic forgetting in neural networks. *PNAS*, 2017.
- [31] Zhizhong Li and Derek Hoiem. Learning without forgetting. *TPAMI*, 2017.
- [32] Rahaf Aljundi, Francesca Babiloni, Mohamed Elhoseiny, Marcus Rohrbach, and Tinne Tuytelaars. Memory aware synapses: Learning what (not) to forget. In *ECCV*, 2018.
- [33] Friedemann Zenke, Ben Poole, and Surya Ganguli. Continual learning through synaptic intelligence. In *ICML*, 2017.
- [34] Sylvestre-Alvise Rebuffi, Alexander Kolesnikov, Georg Sperl, and Christoph H Lampert. icarl: Incremental classifier and representation learning. In *CVPR*, 2017.
- [35] Ameya Prabhu, Philip HS Torr, and Puneet K Dokania. Gdumb: A simple approach that questions our progress in continual learning. In *ECCV*, 2020.
- [36] David Lopez-Paz and Marc’ Aurelio Ranzato. Gradient episodic memory for continual learning. In *NeurIPS*, 2017.
- [37] Yue Wu, Yinpeng Chen, Lijuan Wang, Yuancheng Ye, Zicheng Liu, Yandong Guo, and Yun Fu. Large scale incremental learning. In *CVPR*, 2019.
- [38] Bowen Zhao, Xi Xiao, Guojun Gan, Bin Zhang, and Shu-Tao Xia. Maintaining discrimination and fairness in class incremental learning. In *CVPR*, 2020.
- [39] Jihwan Bang, Heesu Kim, YoungJoon Yoo, Jung-Woo Ha, and Jonghyun Choi. Rainbow memory: Continual learning with a memory of diverse samples. In *CVPR*, 2021.
- [40] Yaoyao Liu, Qianru Sun, and Qianru Sun. Rmm: Reinforced memory management for class-incremental learning. In *NeurIPS*, 2021.

- [41] Elahe Arani, Fahad Sarfraz, and Bahram Zonooz. Learning fast, learning slow: A general continual learning method based on complementary learning system. In *ICLR*, 2022.
- [42] Fahad Sarfraz, Elahe Arani, and Bahram Zonooz. Error sensitivity modulation based experience replay: Mitigating abrupt representation drift in continual learning. In *ICLR*, 2023.
- [43] Decebal Constantin Mocanu, Maria Torres Vega, et al. Online contrastive divergence with generative replay: Experience replay without storing data. *arXiv:1610.05555*, 2016.
- [44] Hanul Shin, Jung Kwon Lee, Jaehong Kim, and Jiwon Kim. Continual learning with deep generative replay. In *NeurIPS*, 2017.
- [45] Chen He, Ruiping Wang, Shiguang Shan, and Xilin Chen. Exemplar-supported generative reproduction for class incremental learning. In *BMVC*, 2018.
- [46] Wenpeng Hu, Zhou Lin, Bing Liu, Chongyang Tao, Zhengwei Tao Tao, Dongyan Zhao, Jinwen Ma, and Rui Yan. Overcoming catastrophic forgetting for continual learning via model adaptation. In *ICLR*, 2019.
- [47] Grégoire Petit, Adrian Popescu, Hugo Schindler, David Picard, and Bertrand Delezoide. Fetrl: Feature translation for exemplar-free class-incremental learning. In *WACV*, 2023.
- [48] Rahaf Aljundi, Punarjay Chakravarty, and Tinne Tuytelaars. Expert gate: Lifelong learning with a network of experts. In *CVPR*, 2017.
- [49] Shipeng Yan, Jiangwei Xie, and Xuming He. Der: Dynamically expandable representation for class incremental learning. In *CVPR*, 2021.
- [50] Fu-Yun Wang, Da-Wei Zhou, Han-Jia Ye, and De-Chuan Zhan. Foster: Feature boosting and compression for class-incremental learning. In *ECCV*, 2022.
- [51] Wenjin Wang, Yunqing Hu, Qianglong Chen, and Yin Zhang. Task difficulty aware parameter allocation & regularization for lifelong learning. In *CVPR*, 2023.
- [52] Da-Wei Zhou, Qi-Wei Wang, Han-Jia Ye, and De-Chuan Zhan. A model or 603 exemplars: Towards memory-efficient class-incremental learning. In *ICLR*, 2023.
- [53] Arun Mallya and Svetlana Lazebnik. Packnet: Adding multiple tasks to a single network by iterative pruning. In *CVPR*, 2018.
- [54] Siavash Golkar, Michael Kagan, and Kyunghyun Cho. Continual learning via neural pruning. In *NeurIPS*, 2019.
- [55] Mitchell Wortsman, Vivek Ramanujan, Rosanne Liu, Aniruddha Kembhavi, Mohammad Rastegari, Jason Yosinski, and Ali Farhadi. Supermasks in superposition. In *NeurIPS*, 2020.
- [56] Aleksandr Dekhovich, David MJ Tax, Marcel HF Sluiter, and Miguel A Bessa. Continual prune-and-select: class-incremental learning with specialized subnetworks. *Applied Intelligence*, 2023.
- [57] Mustafa Burak Gurbuz and Constantine Dovrolis. Nispa: Neuro-inspired stability-plasticity adaptation for continual learning in sparse networks. In *ICML*, 2022.
- [58] Haeyong Kang, Rusty John Lloyd Mina, et al. Forget-free continual learning with winning subnetworks. In *ICML*, 2022.
- [59] Zifeng Wang, Zheng Zhan, Yifan Gong, Geng Yuan, Wei Niu, Tong Jian, Bin Ren, Stratis Ioannidis, Yanzhi Wang, and Jennifer Dy. Sparcl: Sparse continual learning on the edge. In *NeurIPS*, 2022.
- [60] Haeyong Kang, Jaehong Yoon, Sultan Rizky Hikmawan Madjid, Sung Ju Hwang, and Chang D. Yoo. On the soft-subnetwork for few-shot class incremental learning. In *ICLR*, 2023.
- [61] Jie Hu, Li Shen, and Gang Sun. Squeeze-and-excitation networks. In *CVPR*, 2018.
- [62] Kun-Peng Ning, Hai-Jian Ke, Yu-Yang Liu, Jia-Yu Yao, Yong-Hong Tian, and Li Yuan. Sparse orthogonal parameters tuning for continual learning. *arXiv:2411.02813*, 2024.
- [63] Xiao Wang, Tianze Chen, Qiming Ge, Han Xia, Rong Bao, Rui Zheng, Qi Zhang, Tao Gui, and Xuanjing Huang. Orthogonal subspace learning for language model continual learning. *arXiv:2310.14152*, 2023.
- [64] Alex Krizhevsky, Geoffrey Hinton, et al. Learning multiple layers of features from tiny images. 2009.

- [65] Catherine Wah, Steve Branson, Peter Welinder, Pietro Perona, and Serge Belongie. The caltech-ucsd birds-200-2011 dataset. 2011.
- [66] Dan Hendrycks, Steven Basart, Norman Mu, Saurav Kadavath, Frank Wang, Evan Dorundo, Rahul Desai, Tyler Zhu, Samyak Parajuli, Mike Guo, et al. The many faces of robustness: A critical analysis of out-of-distribution generalization. In *ICCV*.
- [67] Dan Hendrycks, Kevin Zhao, Steven Basart, Jacob Steinhardt, and Dawn Song. Natural adversarial examples. In *CVPR*, 2021.
- [68] Yuanhan Zhang, Zhenfei Yin, Jing Shao, and Ziwei Liu. Benchmarking omni-vision representation through the lens of visual realms. In *ECCV*, 2022.
- [69] Xiaohua Zhai, Joan Puigcerver, Alexander Kolesnikov, et al. A large-scale study of representation learning with the visual task adaptation benchmark. *arXiv:1910.04867*, 2019.
- [70] Jia Deng, Wei Dong, Richard Socher, Li-Jia Li, Kai Li, and Li Fei-Fei. Imagenet: A large-scale hierarchical image database. In *CVPR*, 2009.
- [71] Adam Paszke, Sam Gross, Francisco Massa, et al. Pytorch: An imperative style, high-performance deep learning library. In *NeurIPS*. 2019.
- [72] Hai-Long Sun, Da-Wei Zhou, Han-Jia Ye, and De-Chuan Zhan. Pilot: A pre-trained model-based continual learning toolbox. *arXiv:2309.07117*, 2023.

## A Appendix

### A.1 Compared Methods and TOSCA

Here, we provide an overview of the methods evaluated in the main paper. To ensure a fair and consistent basis for comparison, all methods utilize the same PTM. This standardization allows us to isolate the contributions of each method’s unique approach and compare their performance more accurately. Additionally, we present the pseudocode for TOSCA, providing a clear and detailed description of its working algorithm. This helps to better understand how TOSCA operates, offering insights into its efficiency and functionality within the context of class-incremental learning.

**Joint:** This method adheres to the traditional supervised batch learning paradigm, where all classes are presented simultaneously and trained over multiple epochs. It serves as the upper bound for class-incremental learning methods, as it does not experience forgetting.

**Finetune:** This method updates all parameters of the pretrained model when continually trained on new tasks. While it can achieve strong performance, it is susceptible to catastrophic forgetting, where previous knowledge is lost when learning new tasks.

**SimpleCIL** [15]: SimpleCIL uses the PTM in its original form, combined with a prototypical classifier. It constructs a prototype for each class and utilizes a cosine classifier for classification, aiming for efficient task learning without additional adaptations.

**L2P** [12]: L2P integrates visual prompt tuning into class-incremental learning with a pre-trained Vision Transformer (ViT). The method places the prompt only in the initial embedding layer, ensuring that the prompt adjusts the features at the early stage of the model while maintaining the frozen structure of the rest of the pretrained model.

**DualPrompt** [13]: DualPrompt builds on L2P by introducing two types of prompts: general prompts (G-Prompt) and expert prompts (E-Prompt). The G-Prompts are applied to the earlier transformer blocks, allowing for broad task-specific adaptation. E-Prompts, on the other hand, are used in the latter blocks of the transformer, providing more specialized tuning for later stages of task processing. This separation allows for more efficient adaptation.

**CODA-Prompt** [14]: It addresses the challenges of selecting instance-specific prompts by introducing prompt reweighting. It enhances the selection process through an attention mechanism that dynamically weights prompts, improving task-specific performance.

**APER** [15]: This approach builds on SimpleCIL by introducing an adapter to each transformer layer, but only for the initial task. This adapter helps the pre-trained model to extract task-specific features during the first incremental phase, ensuring better adaptation to the new task while minimizing forgetting in subsequent tasks.

**EASE** [16]: This method adds adapters to each transformer layer for every task. This approach leads to good performance by concatenating the feature representations of multiple task-specific backbones, but it comes with an increase in model complexity due to the addition of task-specific adapters at every stage.

**MOS** [17]: It also trains adapters for each transformer layer for every task. However, MOS introduces the concept of adapter merging and replay generation for classifier correction. These processes increase computational complexity, particularly during training, as the model must handle the merging of multiple task-specific adapters with an increasing number of parameters.

---

#### Algorithm 1 TOSCA for PTM-based CIL

---

**Require:** Incremental datasets:  $\{\mathcal{D}^1, \mathcal{D}^2, \dots, \mathcal{D}^B\}$ , Pre-trained embedding:  $\phi(\mathbf{x})$

- 1: **for**  $b = 1, 2, \dots, B$  **do**
- 2:   Get the incremental training set  $\mathcal{D}^b$
- 3:   Initialize a new LuCA module  $L_b$  on top of last [CLS] token
- 4:   Optimize the parameters of the module  $L_b$  via Eq. (8)
- 5:   Test the model with all classes seen so far via Eq. (9)
- 6: **end for**

---

## A.2 Additional Results

In this section, we provide a detailed table for pre-trained **ViT-B/16-IN1K** and figures that illustrate each incremental step with **ViT-B/16-IN21K**, showcasing the performance of our proposed method. As demonstrated, our approach consistently achieves superior results in terms of the last incremental accuracy across all datasets. Importantly, this performance improvement is accompanied by a minimal overhead cost during both the training and inference phases, emphasizing the efficiency of our method, and making it highly suitable for real-world applications. Overall, these results underscore the effectiveness of our method in achieving high accuracy while maintaining computational efficiency, positioning it as a competitive solution for class-incremental learning scenarios.

Table A: Average and last accuracy [%] performance on six datasets with **ViT-B/16-IN1K** as the backbone. ‘IN-R/A’ stands for ‘ImageNet-R/A,’ and ‘OmniBench’ stands for ‘OmniBenchmark.’ We report all compared methods with their source code and show the best performance in bold.

Method	CIFAR B0 Inc5		CUB B0 Inc10		IN-R B0 Inc20		IN-A B0 Inc20		OmniBench B0 Inc30		VTAB B0 Inc10	
	$\bar{\mathcal{A}}$	$\mathcal{A}_B$	$\bar{\mathcal{A}}$	$\mathcal{A}_B$	$\bar{\mathcal{A}}$	$\mathcal{A}_B$	$\bar{\mathcal{A}}$	$\mathcal{A}_B$	$\bar{\mathcal{A}}$	$\mathcal{A}_B$	$\bar{\mathcal{A}}$	$\mathcal{A}_B$
Joint	–	95.88 ± 1.0	–	90.19 ± 1.4	–	83.87 ± 1.4	–	74.05 ± 1.9	–	83.08 ± 1.1	–	93.24 ± 1.8
Finetune	44.4 ± 8.4	39.7 ± 6.1	57.27 ± 2.9	34.76 ± 1.1	66.96 ± 3.2	53.64 ± 1.5	28.64 ± 4.5	14.26 ± 1.8	63.35 ± 2.1	45.70 ± 1.0	67.84 ± 4.9	51.12 ± 5.6
SimpleCIL	82.21 ± 0.7	76.24 ± 0.1	90.42 ± 1.4	85.16 ± 0.1	66.89 ± 0.5	61.27 ± 0.1	58.70 ± 1.1	49.44 ± 0.1	78.67 ± 1.4	72.20 ± 0.1	90.50 ± 1.2	83.61 ± 0.1
L2P	83.37 ± 1.7	78.64 ± 1.6	70.64 ± 1.7	58.70 ± 1.1	77.22 ± 0.5	72.35 ± 0.3	52.32 ± 2.2	44.30 ± 0.8	72.76 ± 1.8	63.10 ± 0.6	81.25 ± 3.0	66.71 ± 1.7
DualPrompt	82.41 ± 1.7	76.39 ± 0.6	75.78 ± 2.2	63.47 ± 1.5	74.37 ± 0.5	69.58 ± 2.0	56.42 ± 1.1	46.99 ± 0.3	73.21 ± 1.8	63.63 ± 0.8	82.84 ± 4.7	70.39 ± 5.5
CODA-Prompt	86.67 ± 0.5	80.68 ± 1.1	70.75 ± 1.1	61.61 ± 1.1	78.37 ± 0.5	73.07 ± 0.5	63.61 ± 0.9	52.32 ± 0.4	72.22 ± 0.3	68.26 ± 0.6	84.88 ± 1.1	82.94 ± 1.6
APER-Adapter	88.46 ± 0.8	83.16 ± 0.4	87.64 ± 1.2	80.63 ± 0.1	78.25 ± 0.5	72.07 ± 0.8	66.86 ± 1.3	58.83 ± 0.2	77.66 ± 1.0	70.72 ± 0.4	89.59 ± 1.2	82.60 ± 0.1
EASE	89.94 ± 1.0	84.39 ± 0.6	87.93 ± 1.2	81.00 ± 0.3	82.96 ± 0.3	77.45 ± 0.1	70.49 ± 1.6	62.36 ± 0.5	78.40 ± 0.8	71.60 ± 1.0	90.71 ± 1.6	83.39 ± 0.7
MOS	92.71 ± 1.1	88.82 ± 0.7	<b>92.24</b> ± 0.9	88.02 ± 0.2	83.53 ± 0.7	78.94 ± 0.3	69.14 ± 1.1	61.24 ± 1.8	<b>85.33</b> ± 1.1	78.28 ± 0.5	91.81 ± 0.5	91.77 ± 0.2
TOSCA (ours)	<b>96.03</b> ± 0.9	<b>95.37</b> ± 0.7	91.55 ± 1.8	<b>89.05</b> ± 1.9	<b>83.57</b> ± 0.6	<b>82.25</b> ± 0.6	<b>74.48</b> ± 2.1	<b>72.30</b> ± 1.8	82.48 ± 1.8	<b>78.65</b> ± 1.2	<b>94.33</b> ± 2.0	<b>91.80</b> ± 1.9

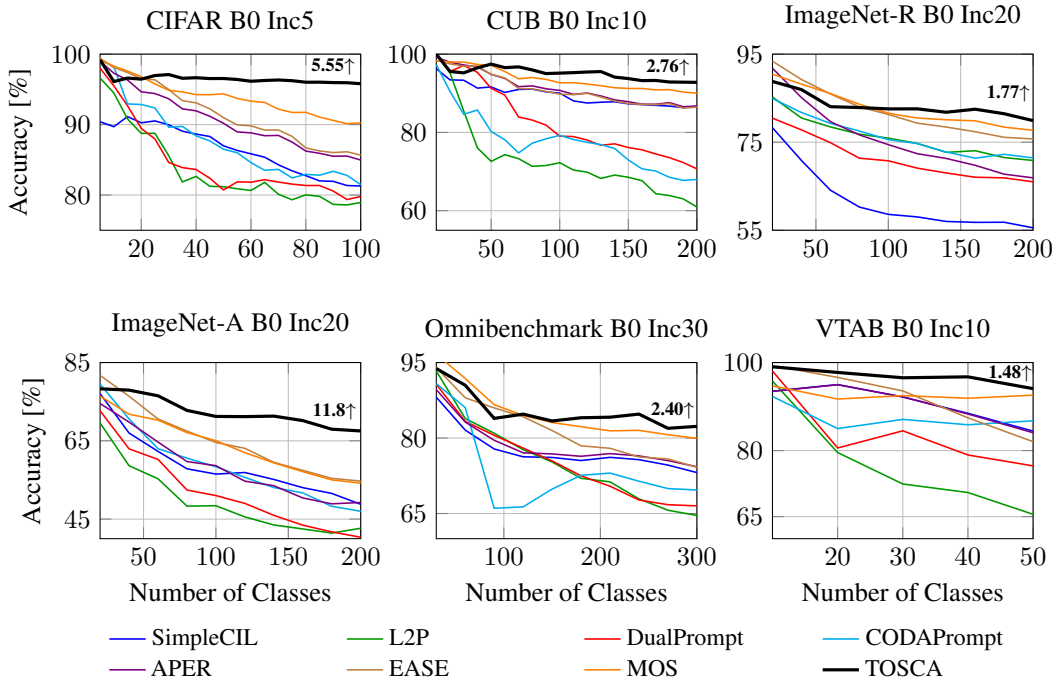


Figure A: Performance curve of different methods on different benchmarks. All methods are initialized with **ViT-B/16-IN21K**. We annotate the relative improvement of TOSCA above the runner-up method with numerical numbers at the last incremental stage.